Astrocytic NKCC1 inhibits seizures by buffering Cl- and antagonizing neuronal NKCC1 at GABAergic synapses

Title: Astrocytic NKCC1 inhibits seizures by buffering Cl^- and antagonizing neuronal NKCC1 at GABAergic synapses

Authors: Trong Dao Nguyen[1], Masaru Ishibashi[1], Adya Saran Sinha[1], Miho Watanabe[1], Daisuke Kato[2], Hiroshi Horiuchi[2], Hiroaki Wake[2], Atsuo Fukuda[1,*]

[1]Department of Neurophysiology, Hamamatsu University School of Medicine, Hamamatsu, 431-3192, Japan.

[2]Department of Anatomy and Molecular Cell Biology, Nagoya University Graduate School of Medicine, Nagoya, 466-8550, Japan.

*Corresponding author. Email: axfukuda@hama-med.ac.jp

One Sentence Summary: NKCC1-mediated high astrocytic $[Cl^-]_i$ plays a pivotal role in seizure prevention at GABAergic tripartite synapses.

Abstract:

A pathological excitatory action of the major inhibitory neurotransmitter γ-aminobutyric acid (GABA) has been observed in epilepsy. Blocking the Cl^- importer NKCC1 with bumetanide is expected to reduce the neuronal intracellular Cl^- concentration ($[Cl^-]_i$) and thereby attenuate the excitatory GABA response. Accordingly, several clinical trials of bumetanide for epilepsy are currently ongoing. Although NKCC1 is expressed in both neurons and glial cells, an involvement of glial NKCC1 in seizures has not yet been reported. Astrocytes maintain high $[Cl^-]_i$ with NKCC1, and this gradient promotes Cl^- efflux via the astrocytic $GABA_A$ receptor ($GABA_AR$). This Cl^- efflux buffers the synaptic cleft Cl^- concentration ($[Cl^-]_o$) to maintain the postsynaptic Cl^- gradient during intense firing of GABAergic neurons, thereby sustaining its inhibitory action during epilepsy. In this study, we investigated the function of astrocytic NKCC1 in modulating the postsynaptic action of GABA in acute seizure models. We used the astrocyte-specific NKCC1 knockout (AstroNKCC1KO) mice. Seizure-like events (SLEs) in CA1 pyramidal neurons *in vitro* and in the *in vivo* pilocarpine-induced seizure model were evaluated. The AstroNKCC1KO mice were prone to seizures with lower threshold and longer duration of SLEs and larger $GABA_AR$-mediated depolarization underlying the SLEs, accompanied by higher Racine-scored seizures. Bumetanide reduced these indicators of seizure in AstroNKCC1KO mice (which still express neuronal NKCC1), but not in the WT, both *in vitro* and *in vivo*. Thus, astrocytic NKCC1 inhibits excitatory GABA-mediated seizures, whereas neuronal NKCC1 has the converse effect, suggesting opposing actions of bumetanide on these cells.

INTRODUCTION

An imbalance between excitatory and inhibitory neurotransmission has been associated with the pathology of epilepsy. In mature neurons, activation of $GABA_AR$ typically mediates Cl^- flow into the cell, resulting in hyperpolarization and the subsequent inhibition of membrane excitability. However, an excitatory action of the primary inhibitory neurotransmitter GABA has been observed in epilepsy *(1-3)*. In seizure-like events (SLEs), hyperactivation of $GABA_AR$ transiently causes intracellular Cl^- accumulation and the collapse of the neuronal Cl^- gradient *(4,5)*. This disruption of Cl^- homeostasis causes a reversal of GABA action, from inhibitory to excitatory. This enhances epileptiform activities during SLEs, and likely underlies the unresponsiveness to first-line benzodiazepine treatment *(2,3)*.

Na^+-K^+-$2Cl^-$ cotransporter type 1 (NKCC1) plays a key role in Cl^- accumulation in neurons *(6)*. Using bumetanide to block the activation of NKCC1 can reduce the $[Cl^-]_i$, and thereby attenuate the excitatory $GABA_AR$ response during epilepsy *(7)*. Bumetanide has been shown to exhibit an anticonvulsant effect in both *in vitro* and *in vivo* experiments *(8-10)*. A recent randomized, double-blind clinical trial showed an additional reduction of neonatal seizure burden by bumetanide over phenobarbital *(11)*. However, in a clinical trial of intravenous bumetanide as an add-on to phenobarbital for the treatment of neonatal seizures, bumetanide did not improve seizure control *(12)*. Consistent with this result, NKCC1 null mice exhibit severe status epilepticus compared with their wild-type (WT) littermates *(13)*. Although these observations suggest that bumetanide inhibits neuronal NKCC1, NKCC1 is expressed not only in neurons, but also in glial cells *(6,14,15)*. The findings in NKCC1 null mice and the off-target effects of bumetanide are therefore difficult to interpret, because the contribution of glial NKCC1 is unclear.

Astrocytes play an important role in synaptic transmission *(16)*. Astrocyte processes tightly enwrap synapses and form a specialized structure called the tripartite synapse *(17,18)*. Astrocytes can respond to synaptically released neurotransmitters, including GABA, via receptors and transporters *(19-22)*. In contrast to $[Cl^-]_i$ in mature neurons (5-10 mM) *(23)*, astrocytic $[Cl^-]_i$ is higher (20–50 mM) that is maintained by NKCC1 activity *(17,24-26)*. Therefore, activation of astrocytic $GABA_AR$ causes Cl^- efflux and depolarizes the astrocytic membrane potential *(22,25)*. Blocking astrocytic gap junction coupling enhances the depolarizing shift of the reversal potential of the inhibitory postsynaptic current evoked by repetitive stimulation of GABAergic neurons, indicative of an astrocytic syncytium-mediated $[Cl^-]_o$ buffering system *(22)*. Recently, optogenetic reduction of astrocytic $[Cl^-]_i$ was shown to suppress inhibitory neurotransmission and enhance neuronal activity, and conversely, optogenetic elevation of astrocytic $[Cl^-]_i$ potentiated inhibitory neurotransmission and reduced neuronal activity, further supporting the existence of an astrocytic syncytium-mediated $[Cl^-]_o$ buffering system *(27)*. The observations suggest that NKCC1-mediated modulation of astrocytic $[Cl^-]_i$ plays a critical role in maintaining $[Cl^-]_o$ and thereby preserving the driving force for inhibitory GABAergic neurotransmission.

In this study, we investigated the function of astrocytic NKCC1 in GABA switching, based on astrocytic $GABA_AR$-mediated spatial Cl^- buffering in an epilepsy model. We used the Cre-loxP system to specifically delete NKCC1 in astrocytes to reduce their ability to modulate Cl^- levels. We found that mice lacking astrocytic NKCC1 were more susceptible to evoked seizures in both *in vitro* and *in vivo* experiments. The excitatory GABAergic responses were greater, corresponding to astrocytic $[Cl]_i$ reduction, suggesting that NKCC1 and net astrocytic Cl^- efflux play critical roles in GABA functional switching during epileptic seizures. Because astrocytic and neuronal NKCC1 play opposing roles in $GABA_AR$-mediated seizures, the clinical use of bumetanide could be a double-edged sword.

RESULTS

Astrocytic $GABA_AR$-mediated Cl^- flux is reversed in AstroNKCC1KO mice

NKCC1 plays a critical role in modulating the high $[Cl^-]_i$ in astrocytes in the hippocampus *(25)*. Therefore, using the Cre-loxP system, we specifically depleted NKCC1 in astrocytes (Fig. 1A). To examine whether astrocytes were deficient in NKCC1, we performed double staining for NKCC1 and GFAP in the hippocampus (Fig. 1B). A clear reduction in the colocalization of NKCC1 and GFAP was observed in AstroNKCC1KO slices (0.01 ± 0.002) compared with WT slices (0.396 ± 0.023, $P < 0.001$; Fig. 1C).

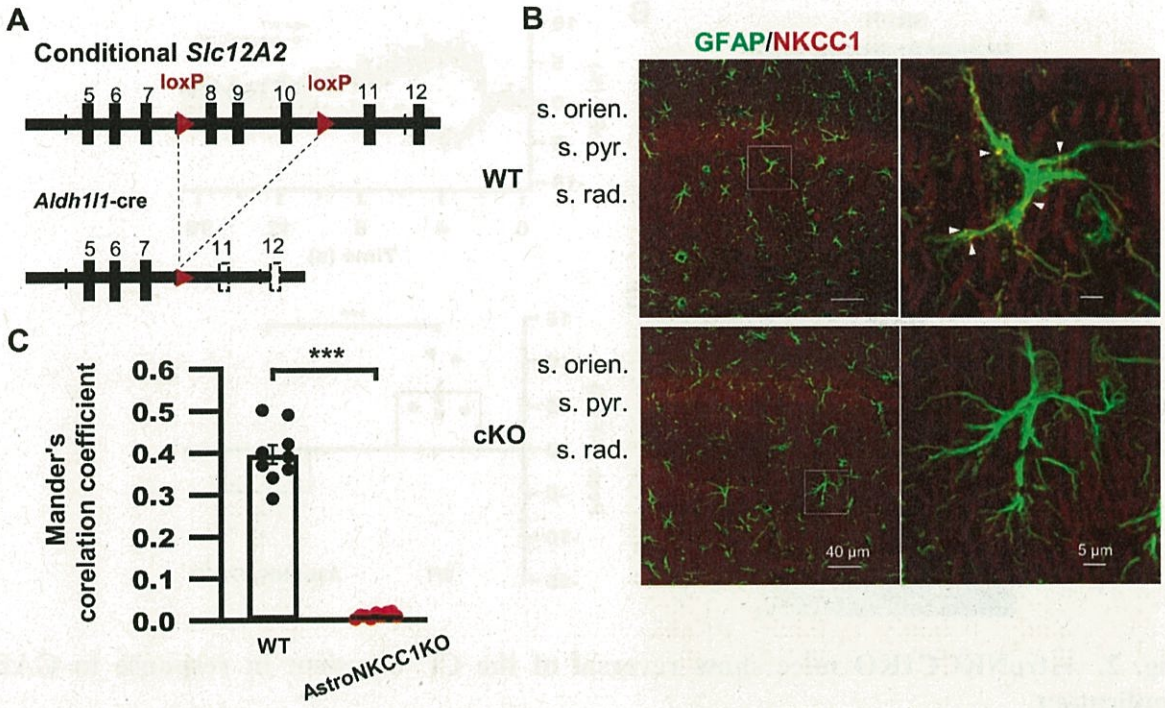

Fig. 1. Conditional depletion of NKCC1 from astrocytes.
A. In the targeted *Slc12a2* locus, exons 8–10 are flanked by loxP sites. Cre-dependent recombination with the astrocyte promoter *Aldh1l1* causes a frameshift (dotted exons) and introduces a stop codon in exon 12. **B**. Representative confocal images showing hippocampal CA1 stratum radiatum astrocytic GFAP and NKCC1 immunoreactivities in WT and AstroNKCC1KO mice. Arrowheads indicate colocalization of NKCC1 and GFAP **C.** Quantitative evaluation of the colocalization of GFAP and NKCC1 using Manders' correlation coefficient. The NKCC1 overlap area is expressed as a percentage of the GFAP-immunoreactive area. Student's *t*-test, ***$P <$ 0.001. Bars show the mean ± SEM with superimposed individual experiment points for the WT group (black, $n = 9$ slices from 3 mice) and the AstroNKCC1KO group (red, $n = 9$ slices from 3 mice). s. orien.: stratum oriens; s.pyr.: stratum pyramydale; s. rad.: stratum radiatum.

To examine whether the depletion of NKCC1 from astrocytes caused a reduction in astrocytic $[Cl^-]_i$, we measured changes in the fluorescence intensity of the Cl^- indicator MQAE during GABA puff application (Fig. 2A). Under normal conditions of high astrocytic $[Cl^-]_i$, with positive Cl^- reversal potential to resting membrane potential (Vrest) in WT mice, local puff application of GABA (1 mM) increased the ΔF/F of MQAE (6.7 ± 3.1, $n = 6$ cells), indicating astrocytic $[Cl^-]_i$ decrease or Cl^- efflux. However, in AstroNKCC1KO astrocytes, GABA puff reduced the ΔF/F of MQAE (−4.9 ± 2.0, $n = 6$ cells), indicating astrocytic $[Cl^-]_i$ increase or Cl^- influx ($P < 0.001$, Student's *t*-test; Fig. 2B, C). These results reveal low astrocytic $[Cl^-]_i$ caused by depletion of astrocytic NKCC1 in AstroNKCC1KO mice.

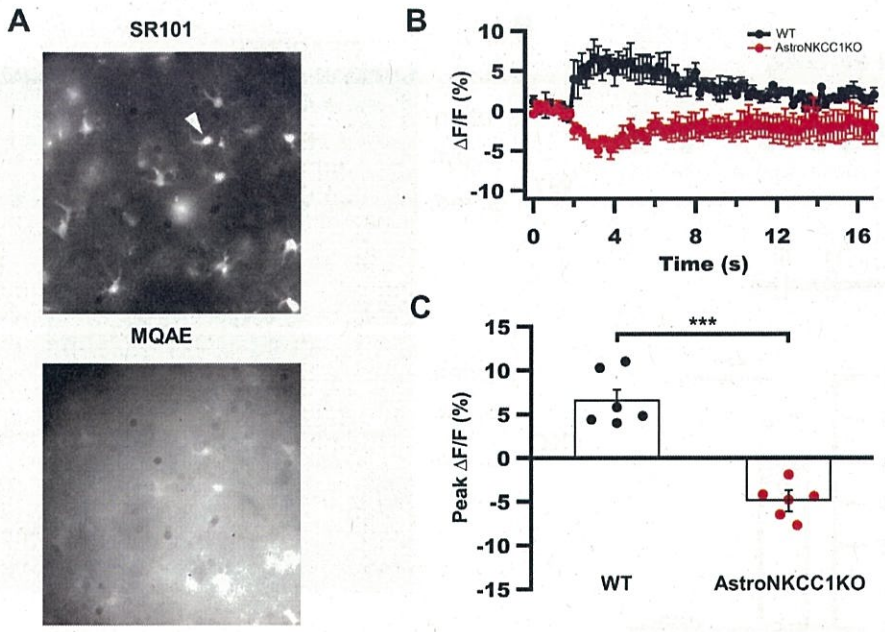

Fig. 2. AstroNKCC1KO mice show reversal of the Cl^- transient in response to GABA application.

A. Fluorescence images of astrocytes labeled with SR101 and the Cl^- indicator MQAE taken from the CA1 stratum radiatum of an acute hippocampal slice. The arrowhead indicates the examined astrocyte (scale bar: 10 μm). **B.** Histogram shows the mean ± SEM of the Cl^- transient (ΔF/F) induced by pressure application of GABA (1 mM for 1 s) in the soma of an astrocyte. Note that the Cl^- response was reversed in AstroNKCC1KO mice compared with WT mice. Graph shows the mean ± SEM. **C.** Peak ΔF/F responses to GABA application in WT and AstroNKCC1KO neurons. Error bars show the mean ± SEM with superimposed individual experimental points for the WT group (black) and the AstroNKCC1KO group (red) (Student's *t*- test, *** $P < 0.001$).

AstroNKCC1KO neurons are prone to SLEs.

To compare the SLE susceptibility between WT and AstroNKCC1KO neurons, the intensity of tetanic stimulation was increased from 50 μA to 450 μA, with 100 μA increments. The event was considered as an SLE when it exhibited seizure-like after-discharge (see Material and Methods). The minimum stimulation intensity for triggering SLE was recorded as the SLE threshold (Fig. 3A). In CA1 pyramidal WT neurons, the induction intensity threshold was 325.0 ± 41.2 μA (n = 8 cells; Fig. 3B). In comparison, in CA1 pyramidal AstroNKCC1KO neurons, the SLE threshold was 121.4 ± 18.4 μA (n = 7 cells). Thus, the threshold for triggering SLEs was significantly reduced in AstroNKCC1KO neurons ($P < 0.01$; Fig. 3B). In addition, the SLE in AstroNKCC1KO neurons lasted longer with the same stimulus intensity, with the duration (19.6 ± 1.6 s, $n = 7$ cells) being significantly longer than in WT neurons (9.1 ± 1.3 s, $n = 8$ cells) at 450 μA ($P < 0.001$; Fig. 3C). These results indicate that AstroNKCC1KO neurons were more susceptible to seizure than WT neurons.

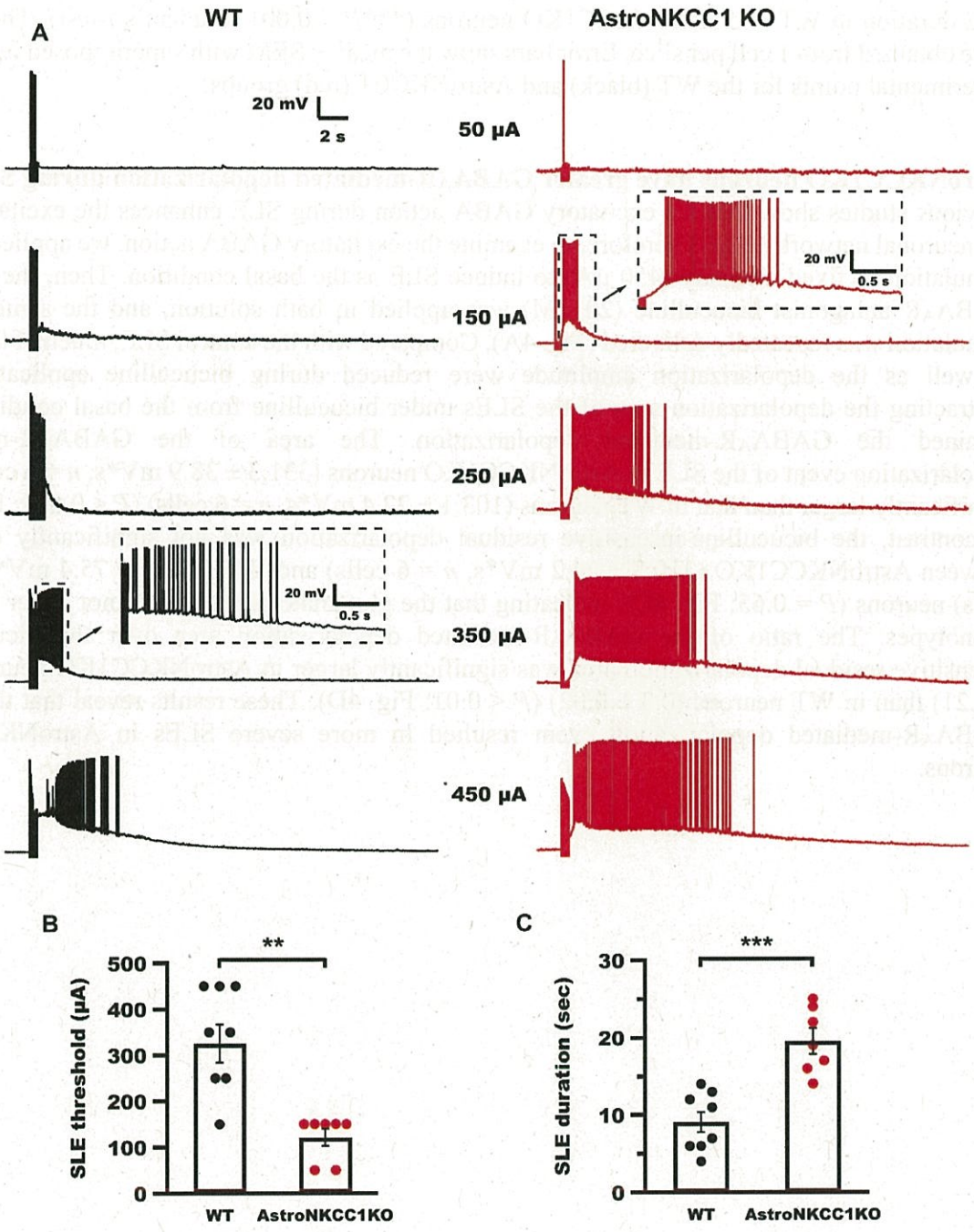

Fig. 3. AstroNKCC1KO neurons are prone to seizure compared with WT neurons.
A. Representative responses of CA1 pyramidal neuron membrane potentials to step-wise amplitude increases of tetanic stimulation. Inset of expanded traces show action potentials occurring on the decay phase of the large depolarization period. The amplitude of this step-wise stimulation was considered the SLE threshold (see Materials and Methods) **B.** Mean of SLE threshold in WT and AstroNKCC1KO neurons (**$P < 0.01$, Mann–Whitney *U*-test). **C.** Mean of

SLE duration in WT and AstroNKCC1KO neurons (***$P < 0.001$, Student's t-test). The results were obtained from 1 cell per slice. Error bars show the mean ± SEM with superimposed individual experimental points for the WT (black) and AstroNKCC1 (red) groups.

AstroNKCC1KO neurons have greater $GABA_AR$-mediated depolarization during SLE. Previous studies show that the excitatory GABA action during SLE enhances the excitability of the neuronal network *(2-5)*. Therefore, to examine the excitatory GABA action, we applied tetanic stimulation of fixed intensity (450 μA) to induce SLE as the basal condition. Then, the specific $GABA_AR$ antagonist bicuculline (20 μM) was applied in bath solution, and the same tetanic stimulation was repeatedly delivered (Fig. 4A). Compared with the control SLE, much of the firing as well as the depolarization amplitude were reduced during bicuculline application. By subtracting the depolarization area of the SLEs under bicuculline from the basal condition, we obtained the $GABA_AR$-mediated depolarization. The area of the $GABA_AR$-mediated depolarization event of the SLE in AstroNKCC1KO neurons (331.3 ± 38.9 mV*s, $n = 6$ cells) was significantly larger than that in WT neurons (103.1 ± 22.4 mV*s, $n = 6$ cells) ($P < 0.001$; Fig. 4B). In contrast, the bicuculline-insensitive residual depolarization was not significantly different between AstroNKCC1KO (310.3 ± 74.2 mV*s, $n = 6$ cells) and WT (359.6 ± 75.4 mV*s, $n = 6$ cells) neurons ($P = 0.65$; Fig. 4C), indicating that the glutamatergic input did not differ between phenotypes. The ratio of the $GABA_AR$-mediated depolarization area over the bicuculline-insensitive residual depolarization area was significantly larger in AstroNKCC1KO neurons (1.3 ± 0.21) than in WT neurons (0.3 ± 0.02) ($P < 0.01$; Fig. 4D). These results reveal that the larger $GABA_AR$-mediated depolarization event resulted in more severe SLEs in AstroNKCC1KO neurons.

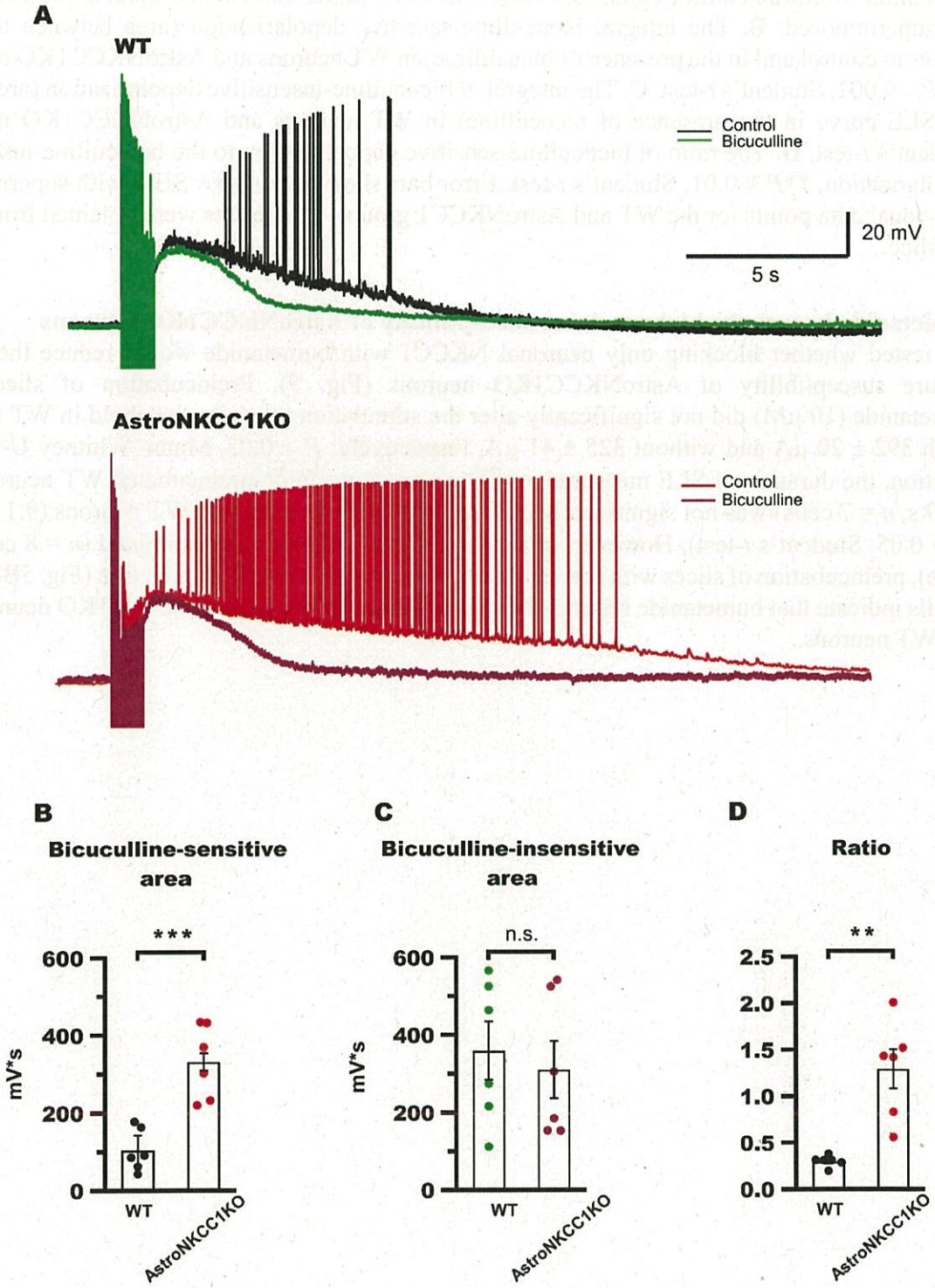

Fig. 4. GABA$_A$R-mediated depolarization during SLEs is greater in AstroNKCC1KO mice. **A.** Representative SLEs from WT neurons (left) and AstroNKCC1KO neurons (right) under control conditions or during GABA$_A$R blockade by bicuculline. The GABA$_A$R-mediated depolarization was obtained by digital subtraction of the area under the curve in the presence of

bicuculline from the control condition. Note that SLEs under control and bicuculline conditions are superimposed. **B.** The integral bicuculline-sensitive depolarization (area between the SLE curves in control and in the presence of bicuculline) in WT neurons and AstroNKCC1KO neurons. ***$P < 0.001$, Student's *t*-test. **C.** The integral of bicuculline-insensitive depolarization (area under the SLE curve in the presence of bicuculline) in WT neurons and AstroNKCC1KO neurons. Student's *t*-test. **D.** The ratio of bicuculline-sensitive depolarization to the bicuculline-insensitive depolarization. **$P < 0.01$, Student's *t*-test. Error bars show the mean ± SEM with superimposed individual data points for the WT and AstroNKCC1 groups. The results were obtained from 1 cell per slice.

Bumetanide lessens the higher seizure susceptibility of AstroNKCC1KO neurons

We tested whether blocking only neuronal NKCC1 with bumetanide would reduce the higher seizure susceptibility of AstroNKCC1KO neurons (Fig. 5). Preincubation of slices with bumetanide (10 μM) did not significantly alter the stimulation intensity threshold in WT neurons (with 392 ± 20 μA and without 325 ± 41 μA, respectively; $P > 0.05$, Mann–Whitney *U*-test). In addition, the duration of SLE measured at 450 μA in bumetanide-preincubated WT neurons (8.8 ± 0.9 s, $n = 7$ cells) was not significantly different from that in untreated WT neurons (9.1 ± 1.3 s) ($P > 0.05$, Student's *t*-test). However, in all AstroNKCC1KO neurons examined ($n = 8$ cells in 3 mice), preincubation of slices with bumetanide completely blocked SLE induction (Fig. 5B). These results indicate that bumetanide reduces the higher susceptibility in AstroNKCC1KO neurons, but not WT neurons.

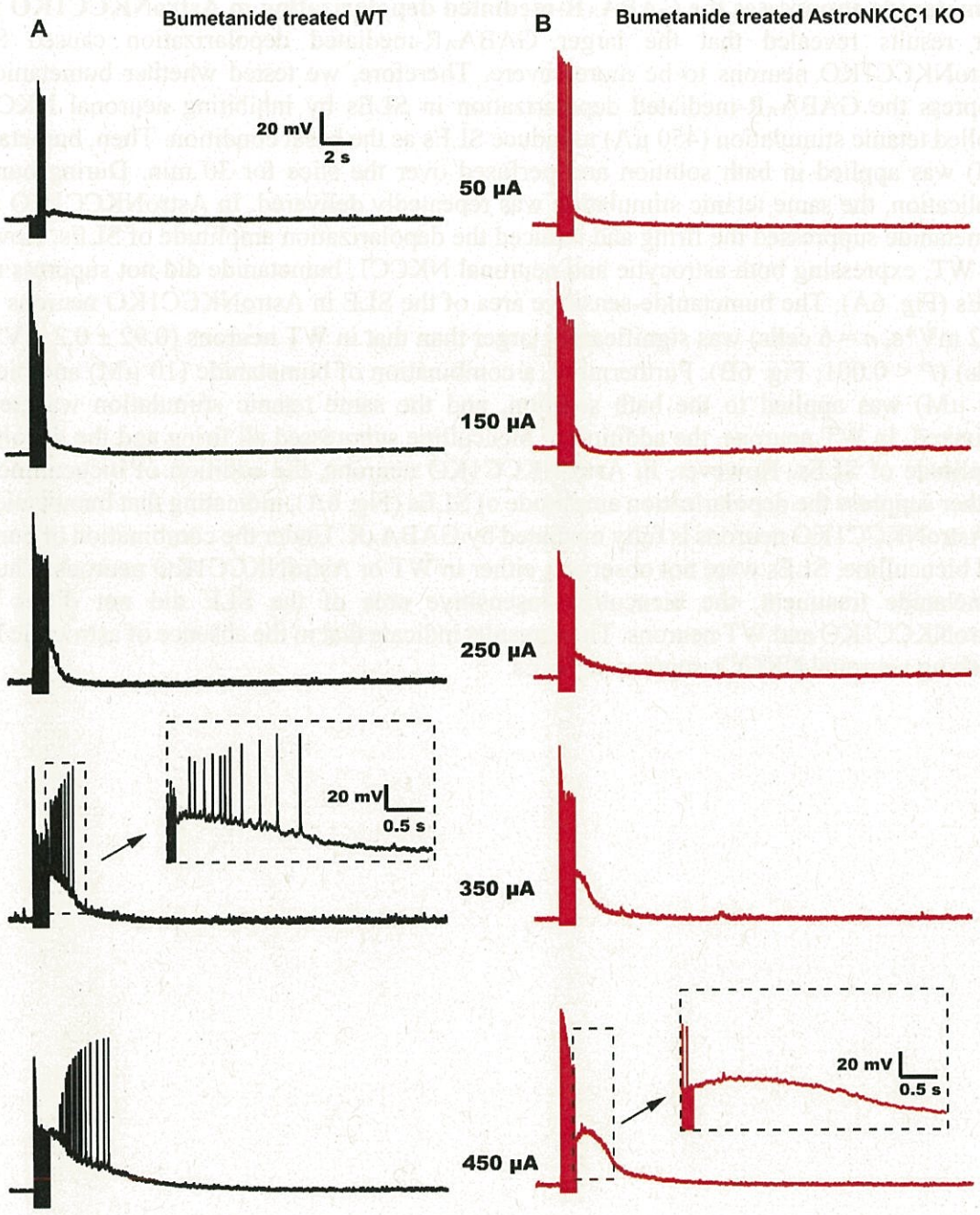

Fig. 5. Bumetanide lessens the higher seizure susceptibility in AstroNKCC1KO neurons
Representative responses of CA1 pyramidal neuron membrane potentials to step-wise amplitude increases of tetanic stimulation in bumetanide-treated WT neurons **(A)** and AstroNKCC1KO neurons **(B).** Inset of expanded traces show action potentials on the decay phase of the large depolarization period. Note that action potentials were absent on the decay phase of the depolarization in bumetanide-treated AstroNKCC1KO neurons.

Bumetanide suppresses the $GABA_AR$-mediated depolarization in AstroNKCC1KO mice

Our results revealed that the larger $GABA_AR$-mediated depolarization caused SLEs in AstroNKCC1KO neurons to be more severe. Therefore, we tested whether bumetanide could suppress the $GABA_AR$-mediated depolarization in SLEs by inhibiting neuronal NKCC1. We applied tetanic stimulation (450 μA) to induce SLEs as the basal condition. Then, bumetanide (10 μM) was applied in bath solution and perfused over the slice for 30 min. During bumetanide application, the same tetanic stimulation was repeatedly delivered. In AstroNKCC1KO neurons, bumetanide suppressed the firing and reduced the depolarization amplitude of SLEs. However, in the WT, expressing both astrocytic and neuronal NKCC1, bumetanide did not suppress neuronal SLEs (Fig. 6A). The bumetanide-sensitive area of the SLE in AstroNKCC1KO neurons (326.6 ± 23.2 mV*s, $n = 6$ cells) was significantly larger than that in WT neurons (0.92 ± 0.2 mV*s, $n = 6$ cells) ($P < 0.001$; Fig. 6B). Furthermore, a combination of bumetanide (10 μM) and bicuculline (20 μM) was applied to the bath solution, and the same tetanic stimulation was repeatedly delivered. In WT neurons, the addition of bicuculline suppressed all firing and the depolarization amplitude of SLEs. However, in AstroNKCC1KO neurons, the addition of bicuculline did not further suppress the depolarization amplitude of SLEs (Fig. 6A), indicating that bumetanide action in AstroNKCC1KO neurons is fully mediated by $GABA_AR$. Under the combination of bumetanide and bicuculline, SLEs were not observed, either in WT or AstroNKCC1KO neurons. Thus, under bumetanide treatment, the bicuculline-insensitive area of the SLE did not differ between AstroNKCC1KO and WT neurons. These results indicate that in the absence of astrocytic NKCC1, blocking neuronal NKCC1 suppresses SLEs.

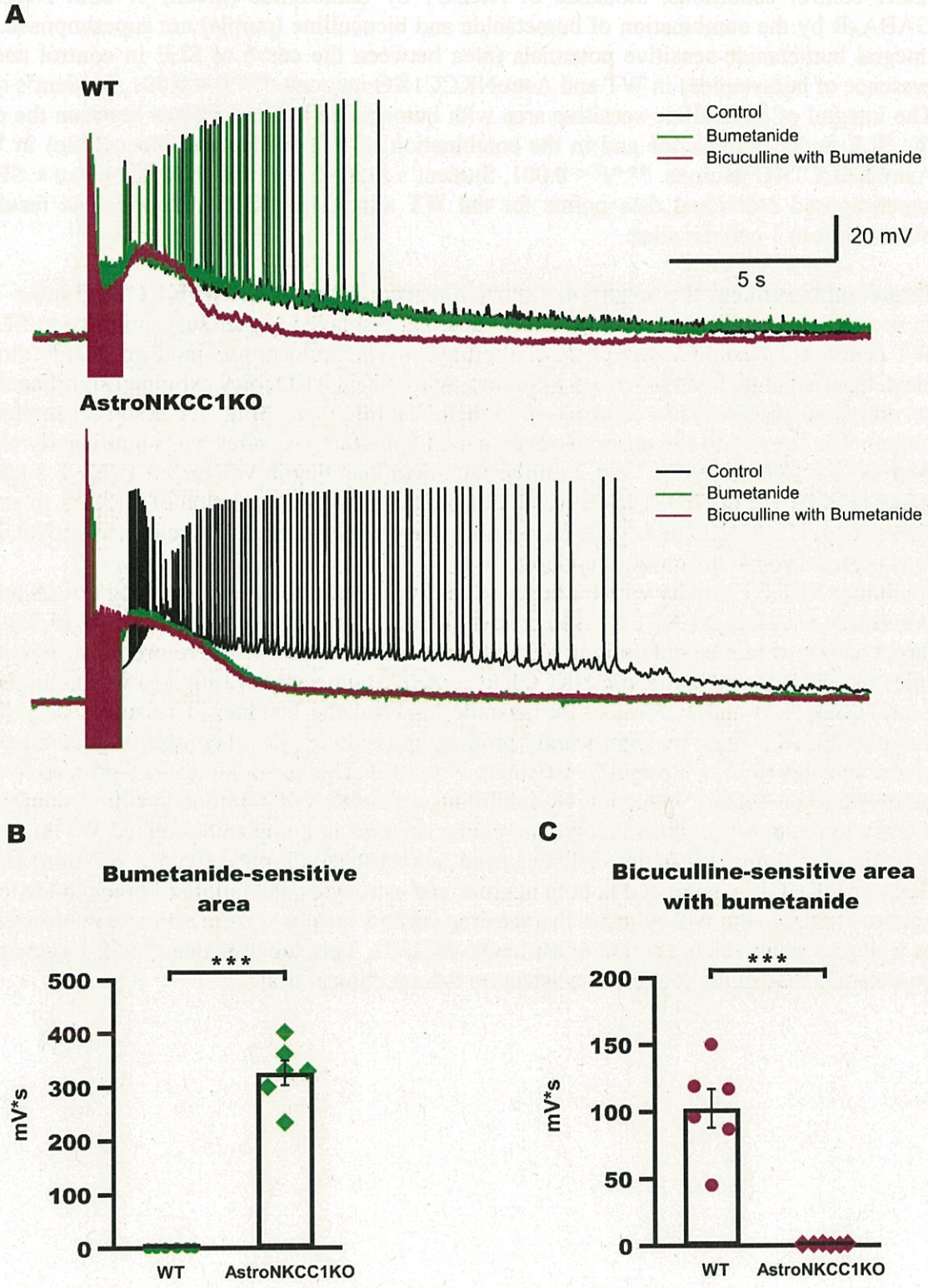

Fig. 6. Bumetanide suppresses SLEs in AstroNKCC1KO neurons

A. Representative SLE obtained from WT neurons (upper) and AstroNKCC1KO neurons (lower) under control conditions; blockade of NKCC1 by bumetanide (green) or both NKCC1 and $GABA_AR$ by the combination of bumetanide and bicuculline (purple) are superimposed. **B.** The integral bumetanide-sensitive potentials (area between the curve of SLE in control and in the presence of bumetanide) in WT and AstroNKCC1KO neurons. ***$P < 0.001$, Student's *t*-test. **C.** The integral of bicuculline-sensitive area with bumetanide treatment (area between the curve of the SLE under bumetanide and in the combination of bumetanide and bicuculline) in WT and AstroNKCC1KO neurons. ***$P < 0.001$, Student's *t*-test. Error bars show the mean ± SEM with superimposed individual data points for the WT and AstroNKCC1 groups. The results were obtained from 1 cell per slice.

Bumetanide reduces the heightened seizure susceptibility in AstroNKCC1KO mice

In *in vitro* experiments, AstroNKCC1KO neurons displayed higher susceptibility to SLEs than WT neurons. To examine seizure susceptibility *in vivo*, a pilocarpine-induced seizure model was used. Consistent with the *in vitro* preparation, AstroNKCC1KO mice exhibited significantly more severe seizure behaviors in comparison to their WT littermates (Fig. 7A; also see supplementary video). The latency to the onset of generalized tonic-clonic seizures was significantly shorter in AstroNKCC1KO mice (70.7 ± 1.2 min, $n = 6$ mice) than that in WT mice (95.5 ± 6.2 min, $n = 6$ mice) ($P < 0.01$; Fig. 7B). These results indicate that selective depletion of NKCC1 in astrocytes cause AstroNKCC1KO mice to be susceptible to epileptic seizures. Therefore, astrocytic NKCC1 may protect against the onset of epilepsy.

Inhibiting NKCC1 activity with bumetanide has been shown to have conflicting effects on seizure prevention *(7)*. Because NKCC1 is expressed in both neurons and astrocytes *(6,14,15,26)*, the off-target action of bumetanide might account for the inconsistency. Therefore, to differentiate the roles of neuronal and astrocytic NKCC1 in seizures, bumetanide (2 mg/kg) was administered to AstroNKCC1KO and WT mice. Bumetanide lessened the heightened seizure susceptibility of AstroNKCC1KO mice by significantly prolonging the latency to the onset of generalized tonic-clonic seizures (93.7 ± 2.8 min, $n = 6$ mice, $P < 0.01$). This result indicates a protective effect of bumetanide on seizure induction by inhibiting neuronal NKCC1 function. In comparison, the latency to the onset of generalized tonic-clonic seizures in bumetanide-treated WT mice (97.0 ± 5.3 min, $n = 6$ mice) was not different from non-treated WT mice (95.5 ± 6.2 min) (Fig. 7B). Because NKCC1 is expressed in both neurons and astrocytes, the failure of bumetanide to protect against seizure in the WT indicates that the drug inhibits the pro-seizure action of neuronal NKCC1 as well as the anti-seizure action of astrocytic NKCC1. This suggests that the off-target actions of bumetanide may underlie the inconsistencies among clinical trials.

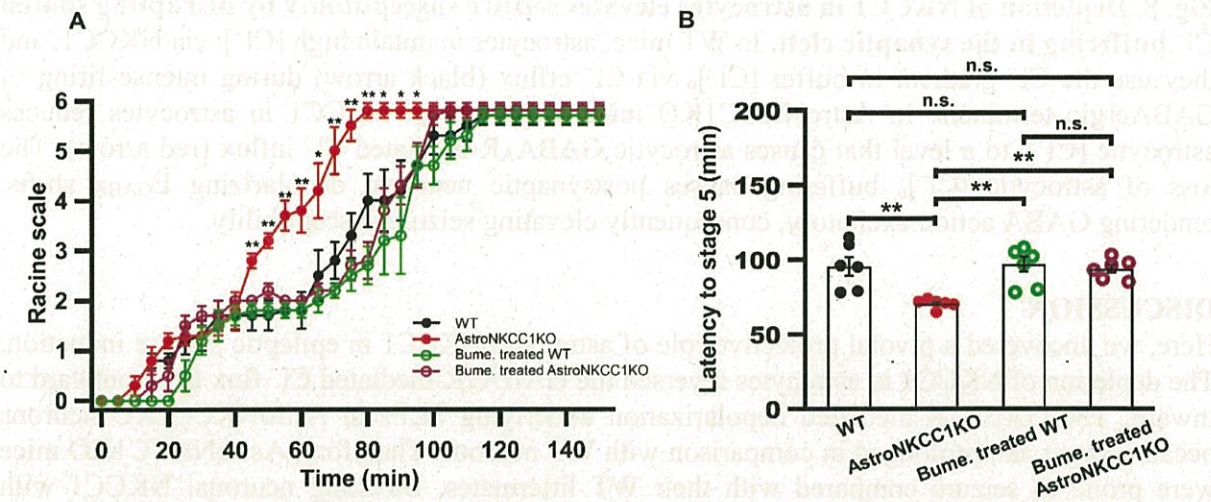

Fig. 7. AstroNKCC1KO mice are prone to seizures.
A. Temporal changes in the mean Racine scale score in WT, AstroNKCC1KO, bumetanide-treated WT and bumetanide-treated AstroNKCC1KO mice. The first pilocarpine treatment was given at time 0. The error bar represents the mean ± SEM (Kruskal–Wallis test, $*P < 0.05$, $**P < 0.01$, 6 mice per group) **B.** Mean latency to stage 5 Racine scale score in WT, AstroNKCC1KO, bumetanide-treated WT and bumetanide-treated AstroNKCC1KO mice. One-way ANOVA, followed by Bonferroni *post hoc*-test, $**P < 0.01$. Error bars show the mean ± SEM with superimposed individual data points for WT (black closed circle), AstroNKCC1KO (red closed circle), bumetanide-treated WT (green open circle) and bumetanide-treated AstroNKCC1KO (brown open circle) mice. Bume.: Bumetanide.

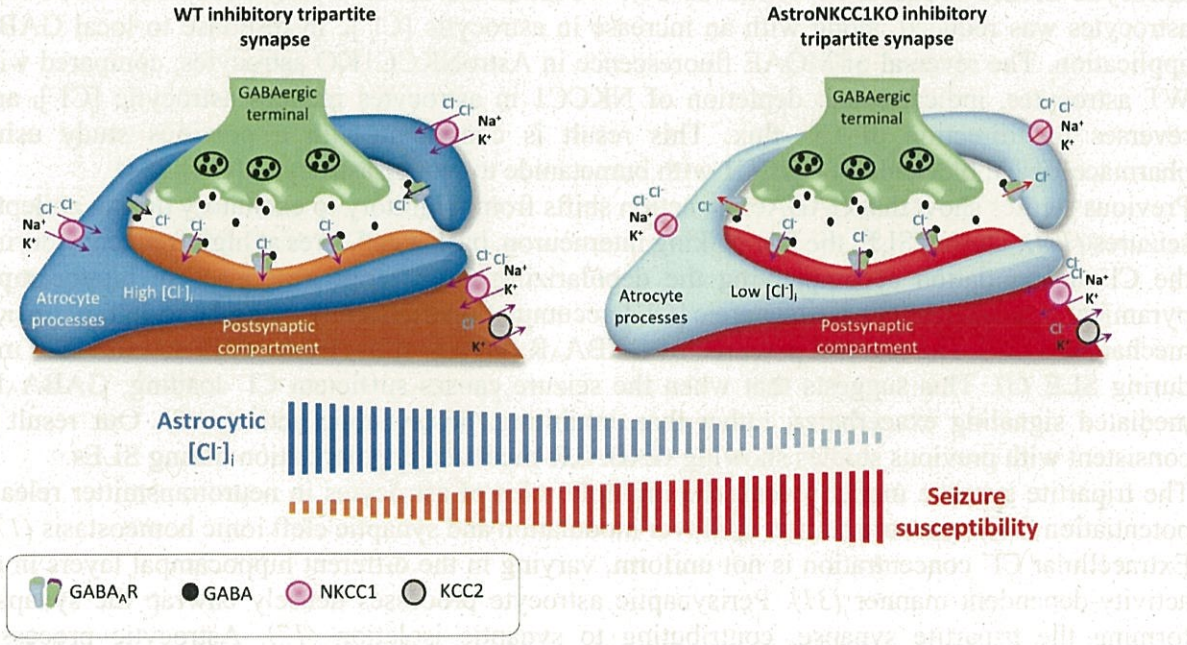

Fig. 8. Depletion of NKCC1 in astrocytes elevates seizure susceptibility by disrupting spatial Cl^- buffering in the synaptic cleft. In WT mice, astrocytes maintain high $[Cl^-]_i$ via NKCC1, and they use the Cl^- gradient to buffer $[Cl^-]_o$ via Cl^- efflux (black arrow) during intense firing of GABAergic terminals. In AstroNKCC1KO mice, depletion of NKCC1 in astrocytes reduces astrocytic $[Cl^-]_i$ to a level that causes astrocytic $GABA_AR$-mediated Cl^- influx (red arrow). The loss of astrocytic $[Cl^-]_o$ buffering causes postsynaptic neuronal depolarizing E_{GABA} shifts, rendering GABA action excitatory, consequently elevating seizure susceptibility.

DISCUSSION

Here, we uncovered a pivotal protective role of astrocytic NKCC1 in epileptic seizure induction. The depletion of NKCC1 in astrocytes reversed the $GABA_AR$-mediated Cl^- flux from outward to inward. The $GABA_AR$-mediated depolarization underlying SLEs in AstroNKCC1KO neurons became larger and prolonged in comparison with WT neurons. Therefore, AstroNKCC1KO mice were prone to seizure compared with their WT littermates. Blocking neuronal NKCC1 with bumetanide countered the high seizure susceptibility in AstroNKCC1KO mice, indicating an anti-seizure action on neuronal NKCC1. However, the non-cell-type-selective NKCC1 inhibitor bumetanide did not confer seizure protection in WT mice, indicating that simultaneous inhibition of astrocytic NKCC1 could mask its action on neuronal NKCC1.

NKCC1 plays a major role in modulating the high astrocytic Cl^- concentration *(25-26)*. Therefore, we generated the AstroNKCC1KO mice with specific depletion of NKCC1 in astrocytes to reduce astrocytic $[Cl^-]_i$. Quinoline-based Cl^--sensitive dyes have been widely used to monitor intracellular Cl^- changes. These dyes are insensitive to pH changes *(28)*. It has been shown that changes in pH differ in neurons and astrocytes during SLE *(29)*. Therefore, the pH-insensitivity of these dyes is an advantage. Moreover, using the cell membrane-permeable Cl^- dye MQAE, we minimized the disturbance of astrocytic $[Cl^-]_i$. The direction of $GABA_AR$-mediated Cl^- flow depends on the electrochemical driving force. Because astrocytic $[Cl^-]_i$ is high, activation of astrocytic $GABA_AR$ causes Cl^- efflux *(22-26)*. We found that the $\Delta F/F$ MQAE in AstroNKCC1KO astrocytes was reduced, along with an increase in astrocytic $[Cl^-]_i$, in response to local GABA application. The reversal of MQAE fluorescence in AstroNKCC1KO astrocytes, compared with WT astrocytes, indicates that depletion of NKCC1 in astrocytes reduces astrocytic $[Cl^-]_i$ and reverses the direction of Cl^- flux. This result is consistent with a previous study using pharmacological blockade of NKCC1 with bumetanide to reduce astrocytic $[Cl^-]_i$ *(26)*.

Previous studies show that GABAergic action shifts from inhibitory to excitatory during epileptic seizures *(1-4)*. During SLE, the fast-spiking interneuron, basket cell, fires at high frequency during the Cl^- accumulation accompanying the depolarizing GABAergic responses in hippocampal pyramidal neurons *(2)*. The postsynaptic $[Cl^-]_i$ accumulation transiently overwhelms Cl^- extrusion mechanisms *(30)*. The reversal potential of $GABA_AR$ (E_{GABA}) shifts from −83.9 mV to −42.7 mV during SLE *(3)*. This suggests that when the seizure causes sufficient Cl^- loading, $GABA_AR$-mediated signaling exacerbates, rather than inhibiting, postsynaptic activity *(3)*. Our result is consistent with previous studies showing $GABA_AR$-mediated depolarization during SLEs.

The tripartite synapse model reveals the multiple roles of astrocytes in neurotransmitter release potentiation *(16)*, neurotransmitter spillover modulation and synaptic cleft ionic homeostasis *(17)*. Extracellular Cl^- concentration is not uniform, varying in the different hippocampal layers in an activity-dependent manner *(31)*. Perisynaptic astrocyte processes densely enwrap the synapse, forming the tripartite synapse, contributing to synaptic isolation *(17)*. Astrocytic processes expressing $GABA_AR$ respond to GABA spillover by Cl^- efflux *(22,25)*. Elevation and reduction

of astrocytic $[Cl^-]_i$ enhances and inhibits GABAergic transmission, respectively *(27)*. We found that the amplitude of $GABA_AR$-mediated depolarization during SLE was larger in CA1 pyramidal neurons in AstroNKCC1KO mice than in their WT littermates. This indicates that depletion of NKCC1 from astrocytes reverses astrocytic $GABA_AR$-mediated Cl^- flux from efflux to influx and exacerbates neuronal $GABA_AR$-mediated depolarization during SLE (Fig. 8). Our results support the concept that astrocytic $[Cl^-]_i$ serves as a source of synaptic cleft Cl^- to sustain inhibitory GABAergic transmission *(22, 27)*. It is not yet feasible to directly assess $[Cl^-]_o$ in the synaptic cleft due to technical limitations. However, our current findings suggest that Cl^- buffering plays a pivotal role during SLEs. A recent technical innovation may help confirm our findings *(32)*.

Blocking NKCC1 with bumetanide has been shown to have an anticonvulsant effect both *in vitro* and *in vivo (8-10)*. Furthermore, in clinical a study, bumetanide enhanced the anticonvulsant effect of phenobarbital on neonatal seizure *(11)*. However, the functional role of NKCC1 in epilepsy is still unclear, particularly as NKCC1 null mice exhibit more severe status epilepticus compared with WT mice *(13)*. Furthermore, bumetanide did not show a beneficial effect on neonatal seizure in another clinical trial *(12)*. Notably, our present results demonstrate an ameliorative effect of bumetanide on seizure activities both *in vitro* and *in vivo* in AstroNKCC1KO mice. The AstroNKCC1KO mice were more susceptible to seizures, and blocking neuronal NKCC1 with bumetanide alleviated the symptoms almost completely. Additionally, application of bumetanide in WT mice did not ameliorate seizure severity (Fig. 7). Neuronal NKCC1 theoretically facilitates seizure activity *(8-10)*, and conversely, astrocytic NKCC1 dampens seizure severity, as shown in the present study. The current findings indicate an anti-seizure role of astrocytic NKCC1 and a pro-seizure role of neuronal NKCC1 in acute seizure models. Because systemically administered bumetanide inhibits NKCC1 in both neurons and astrocytes, the differential action of bumetanide on these cell types might underlie the lack of favorable outcome in some clinical trials for epilepsy *(12)* and autism *(33,34)*.

NKCC1 has been suggested to play a role in K^+ uptake in astrocytes under elevated $[K^+]_o$ *(17)*. NKCC1 mediates astrocyte swelling in WT mice under high $[K^+]_o$, but not in NKCC1 null mice, suggesting that the transporter could participate in K^+ clearance in pathological conditions *(35)*. However, another study showed that NKCC1 plays no role in the activity-induced $[K^+]_o$ recovery in hippocampal slices, because blocking NKCC1 with bumetanide had no effect on K^+ clearance *(36)*. Here, astrocytic NKCC1 depletion reversed the Cl^- flux in astrocytes in response to GABA application. Assuming that NKCC1 inwardly co-transports Cl^- and K^+, loss of astrocytic NKCC1 would also disturb $[K^+]_o$ buffering, which could increase seizure susceptibility. However, differences in SLEs between WT and AstroNKCC1KO were $GABA_AR$-dependent, therefore not supporting this concept. Nonetheless, taken together, our findings suggest a key functional role of astrocytic NKCC1 in dampening SLEs.

Our results highlight the importance of high astrocytic $[Cl^-]_i$, sustained by NKCC1, in maintaining $GABA_AR$-mediated inhibitory signal transmission. Our findings suggest that astrocytic $[Cl^-]_i$ serves as a source of $[Cl^-]_o$ in the synaptic cleft via Cl^- efflux through astrocytic $GABA_AR$, itself activated by GABA spillover during SLEs. This, in turn, preserves the Cl^- driving force for postsynaptic neurons, thereby countering the collapse of inhibitory GABAergic transmission. In particular, our findings suggest an anti-seizure action of astrocytic NKCC1, and in contrast, a pro-seizure action of neuronal NKCC1.

In summary, astrocytic NKCC1 plays a pivotal role in seizure prevention, in contrast to the neuronal counterpart. Several clinical trials of bumetanide for the treatment of epilepsy are currently ongoing. The drug is anticipated to reduce the neuronal $[Cl^-]_i$ by inhibiting NKCC1,

thereby maintaining adequate GABAergic inhibition. The dual actions of bumetanide may account for the inconsistencies and the lack of favorable outcome in some clinical trials of the drug.

MATERIALS AND METHODS

Ethical approval

All experiments conformed to the guidelines issued by Hamamatsu University School of Medicine on the ethical use of animals for experimentation.

Animals

Mice were housed in groups of 3–5 in a standard polycarbonate cage on wood shaving bedding under a 12/12-h light-dark cycle (lights on from 7:00 a.m. to 7:00 p.m.). Food and water were provided *ad libitum*. B6;FVB-Tg(Aldh1l1-cre)JD1884Htz/J (Stock No. 023478) mice were purchased from Jackson Laboratories. The NKCC1$^{flox/flox}$ mice used (a gift from Prof. Christian A. Hübner) were as previously described *(37)*. The Aldh1l1-driven conditional NKCC1 knock-out mice were produced by crossbreeding floxed NKCC1 mice with Aldh1l1 promoter-directed Cre recombinase gene-expressing mice. The resulting Aldh1l1$^{Cre/wt}$:NKCC$^{flox/flox}$ mice were compared with their control littermates (Aldh1l1$^{Cre/wt}$:NKCC1$^{wt/wt}$, Aldh1l1$^{wt/wt}$:NKCC1$^{flox/flox}$).

Slice preparation

Acute hippocampal slices were prepared from mice at postnatal day 18 to postnatal day 23. Mice were deeply anesthetized with isoflurane and then decapitated. The brains were quickly removed, and transverse 350-μm slices were cut with a vibratome (7000smz, Campden instruments) using ice-cold, oxygenated ACSF containing the following (in mM): 126 NaCl, 2.5 KCl, 1.25 NaH_2PO_4, 2 $CaCl_2$, 2 $MgSO_4$, 26 $NaHCO_3$, 10 glucose, pH 7.2–7.4. Slices were then incubated for 10 min in an oxygenated N-methyl-D-glucamine (NMDG) recovery solution at room temperature containing the following (in mM): 115 NMDG, 2.5 KCl, 1.2 NaH_2PO_4, 0.5 $CaCl_2$, 10 $MgSO_4$, 25 $NaHCO_3$, 25 glucose (300–306 mOsm). Slices were then carefully rinsed three times and stored for at least 1 h in continuously oxygenated room temperature ACSF.

Electrophysiological recording

Hippocampal slices were transferred to a submerged recording chamber and continuously perfused with oxygenated ACSF. Slices were perfused at 1.5–2 ml/min, and the bath solution was maintained at 30 °C. CA1 pyramidal neurons within the pyramidal cell layer of the hippocampus were visualized under a 40× water immersion objective lens (Nikkon) with an infrared differential contrast filter and targeted for recording. Whole-cell recordings were performed using glass pipettes, pulled from standard wall borosilicate glass pipettes (3–5 MΩ), and containing the following (in mM): 140 K-gluconate, 2 NaCl, 1 $MgCl_2$, 10 HEPES, 0.2 EGTA, 2 Na_2ATP, 0.5 Na_2GTP, pH 7.3–7.4 (with KOH), 300–305 mOsm. Recordings were made using pClamp software, Multiclamp 700B amplifier, and Digidata acquisition board (1550A, Molecular Devices). For identifying astrocytes, slices were incubated in ACSF that contained 100 nM sulforhodamine (SR101, Dojindo) for 30 min at room temperature before recordings *(38)*.

Tetanic stimulation-induced SLEs

SLEs were recorded from CA1 pyramidal neurons in current-clamp mode according to a method described elsewhere *(4)*. In brief, tetanic stimulation (100 Hz for 0.5 s, intensity 450 μA, duration 400 μs) was delivered by a monopolar glass stimulation electrode (0.5–1 MΩ, filled with 2.5 M NaCl) placed in the stratum radiatum. SLEs were characterized by a large membrane potential

depolarization followed by a prolonged train of oscillatory depolarizations (Fig. 3A, inset). In most cells, none or a single action potential occurred in each cycle of oscillatory depolarization. The oscillatory depolarization was dependent on $GABA_AR$ activation and called the seizure-like after-discharge *(4)*. To measure the SLE threshold, the intensity of tetanic stimulation was increased from 50 μA to 450 μA with 100-μA increments at 3-min intervals. In this study, the threshold was considered as the minimal stimulation intensity in which the action potential occurred in cycles of oscillatory depolarization on the decay of the large depolarization phase. Duration of SLEs was measured from the ending of stimulation to the time point when the membrane potential recovers to the baseline with the 450 μA stimulation intensity.

To examine the effect of bumetanide on SLE threshold, the slices were preincubated with bumetanide (10 μM, Sigma-Aldrich) in ACSF for 30 min. The SLE threshold was then measured in the presence of bumetanide (10 μM) in bath solution as described above.

To measure the $GABA_AR$-mediated depolarization during SLEs, the tetanic stimulation (100 Hz for 0.5 s, intensity 450 μA, duration 400 μs) was delivered to trigger SLEs in the control condition. Then, the $GABA_AR$ was completely blocked by applying 20 μM bicuculline (Sigma-Aldrich) in perfused solution, and the same tetanus stimulation was delivered. The SLE depolarization was determined as the area under the SLE curve. The size of the bicuculline-sensitive area was obtained by subtracting the SLE depolarization obtained in the blocker condition from the control condition. Integration of the resulting bicuculline-sensitive area yielded the $GABA_AR$-mediated depolarization during SLE. The bicuculline-insensitive area was determined as the area under the SLE curve in the presence of bicuculline.

To measure the bumetanide and bumetanide + bicuculline-sensitive depolarizations, tetanic stimulation (100 Hz for 0.5 s, intensity 450 μA, duration 400 μs) was delivered to trigger SLEs in the control condition. Then, NKCC1 activation was blocked by applying 10 μM bumetanide to the perfusate for 30 min, and the same intensity of tetanic stimulation was delivered. Then, the combination of bumetanide (10 μM) and bicuculline (20 μM) was applied to the perfusate for 5 min, and the same tetanic stimulation was delivered. The magnitude of the bumetanide-sensitive area was obtained by subtracting the SLE depolarization obtained in the bumetanide condition from the control condition. The magnitude of the bumetanide + bicuculline-sensitive area was obtained by subtracting the SLE depolarization obtained in the bumetanide + bicuculline condition from the bumetanide condition. The integration of the resulting areas yielded the bumetanide-sensitive depolarization and bicuculline-sensitive depolarization, respectively, in the presence of bumetanide during SLE.

MQAE dye-based intracellular Cl^- imaging

The slices were incubated in normal ACSF containing 5 mM of the Cl^--sensitive dye *N*-(ethoxycarbonylmethyl)-6-methoxyquinolinium bromide (MQAE, Dojindo) for 60 min at room temperature. MQAE was excited at 340–380 nm, and its emission, filtered at 435–485 nm, was captured by an EMCCD camera (iXon DV887, Andor). For local GABA pressure application, GABA (1 mM) was added to the ACSF through a glass puff pipette (2–3 MΩ) by pressure injection (30 kPa, 1 s). The tip of the GABA-filled pipette was positioned above the slice within a horizontal distance of 30–60 μm from the recording cells. Changes in MQAE fluorescence were recorded by placing regions of interest over part of the cell soma (5.6 × 5.6 μm) using FIJI (ImageJ). For analysis, background fluorescence was normalized linearly according to the slope for 2 s before GABA application. The index $\Delta F/F$ was used to estimate the relative change in $[Cl^-]_i$; where F is the averaged fluorescence intensity obtained for 2 s before GABA application, and ΔF is the change in F to fluorescence excitation at a given time. Therefore, quenching of the MQAE

fluorescence, corresponding to $[Cl^-]_i$ increase, is expressed as a negative value in this index. An increase in fluorescence intensity over baseline fluorescence ($\Delta F/F$) indicates a relative decrease in $[Cl^-]_i$. In the present study, we did not determine the absolute $[Cl^-]_i$. The experiments were performed at room temperature to reduce leaking of the dye.

Immunohistochemistry

Mice were deeply anesthetized with sodium pentobarbital (50 mg/kg) and transcardially perfused with phosphate-buffered saline (PBS), followed by ice-cold 4% paraformaldehyde (PFA). Brains were removed and placed in 4% PFA overnight, followed by 20% and 30% sucrose in 0.1 M phosphate buffer at 4 °C. Next, brains were frozen, coronally sectioned (20 μm), and processed for immunohistochemistry. Free-floating sections were washed in 0.1 % Tween 20 (Sigma-Aldrich) in PBS (PBS-T), and then blocked using 10% normal goat serum in PBS-T at room temperature. Subsequently, sections were incubated with the primary antibodies (rabbit anti-NKCC1, 1:500, Alomone Lab; chicken anti-GFAP, 1:1,000, Novus Biologicals) diluted in PBS-T at 4 °C for 48 h. The sections were then incubated with secondary antibodies (1:1,000; Alexa Fluor 594 goat anti-rabbit, Invitrogen; 1:1,000, Alexa Fluor 488 goat anti-chicken, Invitrogen) for 2 h at room temperature. After several washes with PBS-T, sections were mounted and cover-slipped. Images were acquired by confocal microscopy (FV1000-D, Olympus). For the assessments, we included three slices from one side of the hippocampus per mouse. The ImageJ program JACoP was used to quantify colocalization by calculating the percentage of colocalization based on Manders' overlapping coefficient *(39,40)*.

Pilocarpine-induced acute seizure model

The ramping-up dosing protocol was used for the preparation of the pilocarpine-induced acute seizure model, according to previously published studies *(41,42)*. In brief, male mice (3–4 months of age) underwent four low-dose treatments by intraperitoneal injection of pilocarpine (100 mg/kg, Wako) every 20 min. WT littermates were always injected together with homozygous AstroNKCC1KO mice, using the same batch of pilocarpine. Thus, there was no systematic difference in pilocarpine injection between WT and AstroNKCC1KO mice. To avoid peripheral cholinergic effects, methyl scopolamine (1 mg/kg; Sigma-Aldrich) was subcutaneously administered 30 min before the application of pilocarpine.

Mice were video recorded during each experiment. Behavioral seizure severity was measured every 5 min, according to a previous study using the Racine scale *(43)*, as follows: Stage 0: no response; Stage 1: facial clonus (blinking, moving, rhythmic chewing); Stage 2: stage 1 plus rhythmic nod; Stage 3: stage 2 plus forelimb myoclonus without upright hind limbs; Stage 4: stage 3 plus upright hind limbs; Stage 5: generalized tonic, a burst of seizure, and loss of control. All mice exhibited stage 5 symptoms on the Racine scale. Animals that died during the experiments were assigned stage 6.

To assess whether blocking NKCC1 with bumetanide suppresses seizures, 2 mg/kg bumetanide (Sigma-Aldrich) was intraperitoneally injected according to a previous study *(10)*. A second dose of bumetanide was administered after 60 min because of its short half-life in brain reported previously *(44)*.

Statistical analysis

The data are reported as mean ± standard error of mean (SEM) for number of cells (n) or mouse preparations, as detailed in the figure legends. Normality test (Shapiro–Wilk test) was applied to the data before running statistical tests. Based on the normality results, data in two sample groups were compared using unpaired Student's t-test or the Mann–Whitney U-test. For the pilocarpine-

induced acute seizure experiment, one-way ANOVA with Bonferroni's multiple comparison test and Kruskal–Wallis test were used. Two-tailed tests were always performed. Statistical differences were established with $P < 0.05$ (*), $P < 0.01$ (**) and $P < 0.001$ (***). Statistical analysis was performed using SPSS statistical software package (SPSS 28 for Windows; SPSS, Inc., Chicago, IL, USA).

List of Supplementary Materials

Movie S1. Pilocarpine-induced seizure behavior in WT mouse

Movie S2. Pilocarpine-induced seizure behavior in AstroNKCC1KO mouse

Movie S3. Pilocarpine-induced seizure behavior in bumetanide-treated WT mouse

Movie S4. Pilocarpine-induced seizure behavior in bumetanide-treated AstroNKCC1KO mouse

Acknowledgments:

We are grateful to Christian A. Hübner (University of Jena, Germany) for the gift of NKCC1$^{flox/flox}$ mice. We thank Barry Patel, PhD, from Edanz (https://jp.edanz.com/ac), for editing a draft of this manuscript.

Funding:

This work was supported by the following:

Ministry of Education, Culture, Sports, Science and Technology of Japan grant for Research on Innovative Areas (Non-linear oscillology), 15H05872 (AF).

Japan Society for the Promotion of Science grant for Scientific Research 17H04025(AF), 21H02661 (AF).

Ministry of Education, Culture, Sports, Science and Technology of Japan grant for Scientific Research on Innovative Areas 21H05687 (AF), 23H04159 (AF).

The Salt Science Research Foundation 2138 (AF).

The Research Grant JERF TENKAN 20002 (MI).

The Hamamatsu University School of Medicine grant-in-aid (TDN).

The Ichiro Kanehara Foundation for living expenses of foreign nationals in Japan (TDN).

Author contributions:

Conceptualization: T.D.N., M.I., A.F.
Methodology: T.D.N., M.I., M.W., A.S.S., H.W., A.F.
Investigation: T.D.N., M.I., A.F.
Visualization: T.D.N., M.I., A.F.
Funding acquisition: T.D.N., M.I., A.F.
Project administration: M.I., A.F.
Supervision: A.F.
Writing – original draft: T.D.N., M.I., A.F.
Writing – review & editing: T.D.N., M.I., M.W., A.S.S., D.K., H.H., H.W., A.F.

Competing interests: The authors declare that the research was conducted in the absence of any commercial or financial relationships that could be constructed as a potential conflict of interest.

References

1. Palma E, Amici M, Sobrero F, Spinelli G, Di Angelantonio S, Ragozzino D, Mascia A, Scoppetta C, Esposito V, Miledi R, Eusebi F. Anomalous levels of Cl^- transporters in the hippocampal subiculum from temporal lobe epilepsy patients make GABA excitatory. *Proc Natl Acad Sci U S A* **103**, 8465-8468 (2006).
2. Isomura Y, Sugimoto M, Fujiwara-Tsukamoto Y, Yamamoto-Muraki S, Yamada J, Fukuda A. Synaptically activated Cl^- accumulation responsible for depolarizing GABAergic responses in mature hippocampal neurons. *J Neurophysiol.* **90**, 2752-2756 (2003).
3. Burman RJ, Selfe JS, Lee JH, van den Berg M, Calin A, Codadu NK, Wright R, Newey SE, Parrish RR, Katz AA, Wilmshurst JM, Akerman CJ, Trevelyan AJ, Raimondo JV. Excitatory GABAergic signalling is associated with benzodiazepine resistance in status epilepticus. *Brain* **142**, 3482-3501 (2019).
4. Fujiwara-Tsukamoto Y, Isomura Y, Nambu A, Takada M. Excitatory GABA input directly drives seizure-like rhythmic synchronization in mature hippocampal CA1 pyramidal cells. *Neuroscience* **119**, 265-275 (2003).
5. Raimondo JV, Burman RJ, Katz AA, Akerman CJ. Ion dynamics during seizures. Front *Cell Neurosci.* **9**, 419 (2015).
6. Yamada J, Okabe A, Toyoda H, Kilb W, Luhmann HJ, Fukuda A. Cl^- uptake promoting depolarizing GABA actions in immature rat neocortical neurones is mediated by NKCC1. *J Physiol.* **557**, 829-841 (2004).
7. Ben-Ari Y. NKCC1 Chloride Importer Antagonists Attenuate Many Neurological and Psychiatric Disorders. *Trends Neurosci.* **40**, 536-554 (2017).
8. Dzhala VI, Talos DM, Sdrulla DA, Brumback AC, Mathews GC, Benke TA, Delpire E, Jensen FE, Staley KJ. NKCC1 transporter facilitates seizures in the developing brain. *Nat Med.* **11**, 1205-1213 (2005).
9. Cleary RT, Sun H, Huynh T, Manning SM, Li Y, Rotenberg A, Talos DM, Kahle KT, Jackson M, Rakhade SN, Berry G, Jensen FE. Bumetanide enhances phenobarbital efficacy in a rat model of hypoxic neonatal seizures. *PLoS One* **8**, e57148 (2013).
10. Sivakumaran S, Maguire J. Bumetanide reduces seizure progression and the development of pharmacoresistant status epilepticus. *Epilepsia* **57**, 222-232 (2016).
11. Soul JS, Bergin AM, Stopp C, Hayes B, Singh A, Fortuno CR, O'Reilly D, Krishnamoorthy K, Jensen FE, Rofeberg V, Dong M, Vinks AA, Wypij D, Staley KJ; Boston Bumetanide Trial Group. A Pilot Randomized, Controlled, Double-Blind Trial of Bumetanide to Treat Neonatal Seizures. *Ann Neurol.* **89**, 327-340 (2021).
12. Pressler RM, Boylan GB, Marlow N, Blennow M, Chiron C, Cross JH, de Vries LS, Hallberg B, Hellström-Westas L, Jullien V, Livingstone V, Mangum B, Murphy B, Murray D, Pons G, Rennie J, Swarte R, Toet MC, Vanhatalo S, Zohar S; Neonatal seizure treatment with Medication Off-patent (NEMO) consortium. Bumetanide for the treatment of seizures in newborn babies with hypoxic ischaemic encephalopathy

(NEMO): an open-label, dose finding, and feasibility phase 1/2 trial. *Lancet Neurol.* **14**, 469-477 (2015).
13. Hampel P, Johne M, Gailus B, Vogel A, Schidlitzki A, Gericke B, Töllner K, Theilmann W, Käufer C, Römermann K, Kaila K, Löscher W. Depletion of the Na-K-2Cl cotransporter NKCC1 results in a more severe epileptic phenotype in the intrahippocampal kainate mouse model of temporal lobe epilepsy. *Neurobiol Dis.* **152**, 105297 (2021).
14. Yan Y, Dempsey RJ, Sun D. Expression of Na(+)-K(+)-Cl(-) cotransporter in rat brain during development and its localization in mature astrocytes. *Brain Res.* **911**, 43-55 (2001)
15. Virtanen MA, Uvarov P, Hübner CA, Kaila K. NKCC1, an Elusive Molecular Target in Brain Development: Making Sense of the Existing Data. *Cells* **9**, 2607 (2020).
16. Perea G, Araque A. Astrocytes potentiate transmitter release at single hippocampal synapses. *Science* **317**, 1083-1086 (2007).
17. Verkhratsky A, Nedergaard M. Physiology of Astroglia. *Physiol Rev.* **98**, 239-389 (2018).
18. Takano T, Wallace JT, Baldwin KT, Purkey AM, Uezu A, Courtland JL, Soderblom EJ, Shimogori T, Maness PF, Eroglu C, Soderling SH. Chemico-genetic discovery of astrocytic control of inhibition in vivo. *Nature.* **588**, 296-302 (2020).
19. Brunskine C, Passlick S, Henneberger C. Structural Heterogeneity of the GABAergic Tripartite Synapse. *Cells* **11**, 3150 (2022).
20. Matos M, Bosson A, Riebe I, Reynell C, Vallée J, Laplante I, Panatier A, Robitaille R, Lacaille JC. Astrocytes detect and upregulate transmission at inhibitory synapses of somatostatin interneurons onto pyramidal cells. *Nat Commun.* **9**: 4254 (2018).
21. Mederos S, Sánchez-Puelles C, Esparza J, Valero M, Ponomarenko A, Perea G. GABAergic signaling to astrocytes in the prefrontal cortex sustains goal-directed behaviors. *Nat Neurosci.* 24, 82-92 (2021).
22. Egawa K, Yamada J, Furukawa T, Yanagawa Y, Fukuda A. Cl^- homeodynamics in gap junction-coupled astrocytic networks on activation of GABAergic synapses. *J Physiol.* **591**, 3901-3917 (2013).
23. Pressey JC, de Saint-Rome M, Raveendran VA, Woodin MA. Chloride transporters controlling neuronal excitability. Physiol Rev. **103**, 1095-1135 (2023).
24. Wilson CS, Mongin AA. The signaling role for chloride in the bidirectional communication between neurons and astrocytes. Neurosci Lett. **689**, 33-44 (2019).
25. Kettenmann H, Backus KH, Schachner M. Gamma-Aminobutyric acid opens Cl^-channels in cultured astrocytes. *Brain Res.* **404**, 1-9 (1987).
26. Engels M, Kalia M, Rahmati S, Petersilie L, Kovermann P, van Putten MJAM, Rose CR, Meijer HGE, Gensch T, Fahlke C. Glial Chloride Homeostasis Under Transient Ischemic Stress. *Front Cell Neurosci.* **15**, 735300 (2021).
27. Untiet V, Beinlich FRM, Kusk P, Kang N, Ladrón-de-Guevara A, Song W, Kjaerby C, Andersen M, Hauglund N, Bojarowska Z, Sigurdsson B, Deng S, Hirase H, Petersen NC, Verkhratsky A, Nedergaard M. Astrocytic chloride is brain state dependent and modulates inhibitory neurotransmission in mice. *Nat Commun.* **14**, 1871 (2023).
28. Arosio D, Ratto GM. Twenty years of fluorescence imaging of intracellular chloride. *Front Cell Neurosci.* **8**, 258 (2014).

29. Raimondo JV, Tomes H, Irkle A, Kay L, Kellaway L, Markram H, Millar RP, Akerman CJ. Tight Coupling of Astrocyte pH Dynamics to Epileptiform Activity Revealed by Genetically Encoded pH Sensors. *J Neurosci.* **36**, 7002-7013 (2016).
30. Wright R, Raimondo JV, Akerman CJ. Spatial and temporal dynamics in the ionic driving force for GABA(A) receptors. *Neural Plast.* **2011**, 728395 (2011).
31. Kroeger D, Tamburri A, Amzica F, Sík A. Activity-dependent layer-specific changes in the extracellular chloride concentration and chloride driving force in the rat hippocampus. *J Neurophysiol.* **103**, 1905-1914 (2010).
32. Kieran P Normoyle, Kevin J Staley. Displacement of extracellular chloride by sulfated glycosaminoglycans of the brain's extracellular matrix. *bioRxiv* (2022).
33. Sprengers JJ, van Andel DM, Zuithoff NPA, Keijzer-Veen MG, Schulp AJA, Scheepers FE, Lilien MR, Oranje B, Bruining H. Bumetanide for Core Symptoms of Autism Spectrum Disorder (BAMBI): A Single Center, Double-Blinded, Participant-Randomized, Placebo-Controlled, Phase-2 Superiority Trial. *J Am Acad Child Adolesc Psychiatry* **60**, 865-876 (2021).
34. Du L, Shan L, Wang B, Li H, Xu Z, Staal WG, Jia F. A Pilot Study on the Combination of Applied Behavior Analysis and Bumetanide Treatment for Children with Autism. *J Child Adolesc Psychopharmacol.* **25**, 585-588 (2015).
35. Su G, Kintner DB, Flagella M, Shull GE, Sun D. Astrocytes from Na(+)-K(+)-Cl(-) cotransporter-null mice exhibit absence of swelling and decrease in EAA release. *Am J Physiol Cell Physiol.* **282**, 1147-1160 (2002).
36. Larsen BR, Assentoft M, Cotrina ML, Hua SZ, Nedergaard M, Kaila K, Voipio J, MacAulay N. Contributions of the Na^+/K^+-ATPase, NKCC1, and Kir4.1 to hippocampal K^+ clearance and volume responses. *Glia* **62**, 608-622 (2014).
37. Antoine MW, Hübner CA, Arezzo JC, Hébert JM. A causative link between inner ear defects and long-term striatal dysfunction. *Science* **341**, 1120-1123 (2013).
38. Nimmerjahn A, Kirchhoff F, Kerr JN, Helmchen F. Sulforhodamine 101 as a specific marker of astroglia in the neocortex in vivo. *Nat Methods.* **1**, 31-37 (2004).
39. Bolte S, Cordelières FP. A guided tour into subcellular colocalization analysis in light microscopy. *J Microsc.* **224**, 213-232 (2006).
40. Dunn KW, Kamocka MM, McDonald JH. A practical guide to evaluating colocalization in biological microscopy. *Am J Physiol Cell Physiol.* **300**, 723-742 (2011).
41. Müller CJ, Gröticke I, Bankstahl M, Löscher W. Behavioral and cognitive alterations, spontaneous seizures, and neuropathology developing after a pilocarpine-induced status epilepticus in C57BL/6 mice. *Exp Neurol.* **219**, 284-297 (2009).
42. Mao XY, Zhou HH, Jin WL. Ferroptosis Induction in Pentylenetetrazole Kindling and Pilocarpine-Induced Epileptic Seizures in Mice. *Front Neurosci.* **13**, 721 (2019).
43. Racine RJ. Modification of seizure activity by electrical stimulation. II. Motor seizure. *Electroencephalogr Clin Neurophysiol.* **32**, 281-294 (1972).
44. Kharod SC, Kang SK, Kadam SD. Off-Label Use of Bumetanide for Brain Disorders: An Overview. *Front Neurosci.* **13**, 310 (2019).